scientific reports

Check for updates

OPEN

The effects and mechanisms of Xiaoyao San on nonalcoholic fatty liver disease rat based on transcriptomics and proteomics analysis

Yunxiao Liu[1,2], Shuanghu Wang[1], Ayesha Younas[1], Jiaojian Lv[1], Abdullah Al Mamun[1] & Chuxiao Shao[1]✉

Nonalcoholic Fatty Liver Disease (NAFLD) is characterized by excessive lipid accumulation in hepatocytes and is closely associated with metabolic disturbances such as obesity, dyslipidemia, and insulin resistance. Despite its increasing prevalence and potential progression to severe liver conditions, there is currently no approved pharmaceutical intervention for NAFLD. Traditional Chinese Medicine (TCM) formulations, such as Xiaoyao San (XYS), have shown therapeutic efficacy in treating NAFLD, but the underlying mechanisms remain unclear. This study employed a multi-omics approach to elucidate the therapeutic mechanisms of XYS in NAFLD. A rat model of NAFLD was established using a high-fat diet (HFD). The chemical constituents of XYS were analyzed using UPLC-MS/MS. Transcriptomics and proteomics analyses were performed to identify potential biological targets and signaling pathways involved in the therapeutic effects of XYS. The results were validated using ELISA and Western blotting. UPLC-MS/MS identified 225 prototype chemical components of XYS in the blood. XYS significantly reduced body weight, liver index, and Lee's index in NAFLD model rats. It ameliorated HFD-induced hepatic steatosis, down-regulated serum levels of ALT, AST, GGT, TG, TC, LDL-C, FBG, IL-1β, IL-6, TNF-α, and ROS, and up-regulated HDL-C levels. Transcriptomics and proteomics analyses revealed that XYS modulated key signaling pathways, including cAMP, TGF-β, NF-κB, and necroptosis. Specifically, XYS down-regulated the expressions of NF-κB, p-NF-κB, FOXO1, TGF-β1, RIP3, and p-MLKL, while up-regulating cAMP, PKA, p-PKA, and PPARα. XYS improves NAFLD by regulating the cAMP/PKA-mediated PPARα, FOXO1, and NF-κB signaling pathways. This study provides a comprehensive understanding of the molecular mechanisms underlying the therapeutic effects of XYS in NAFLD and supports its potential as a novel therapeutic intervention for this condition.

Keywords Xiaoyao San, Nonalcoholic fatty liver disease, Transcriptomics, Proteomics, Signaling Pathway

Abbreviations

ALT	Alanine aminotransferase
AST	Aspartate aminotransferase
BCA	The bicinchoninic acid
BP	Biological processes
cAMP	Cyclic adenosine monophosphate
CC	Cellular components
DEGs	Differentially expressed genes
DEPs	Differentially expressed proteins
ELISA	Enzyme-linked immunosorbent assay

[1]Key Laboratory of Joint Diagnosis and Treatment of Chronic Liver Disease and Liver Cancer of Lishui, The Lishui Hospital of Wenzhou Medical University, The First Affiliated Hospital of Lishui University, Lishui People's Hospital, Lishui, Zhejiang 323000, People's Republic of China. [2]Fourth Clinical Medical College of Xinjiang Medical University, Urumqi, Xinjiang 830000, People's Republic of China. ✉email: scx1818@126.com

FFA	Free fatty acids
FL	Fatty liver
FOXO1	Forkhead box protein O 1
FBG	Fasting blood glucose
GGT	Gamma-glutamyl transferase
GO	Gene Ontology
HCC	Hepatocellular carcinoma
HDL-C	High-density lipoprotein cholesterol
H&E	Hematein-Eosin
HFD	High-fat diet
IL-1β	Interleukin-1β
IL-6	Interleukin-6
IR	Insulin resistance
KEGG	The Kyoto Encyclopedia of Genes and Genomes
LDL-C	Low-density lipoprotein cholesterol
MF	Molecular composition
NAFLD	Nonalcoholic fatty liver disease
NASH	Nonalcoholic steatohepatitis
NF-κB	Nuclear factor-kappa B
PCA	Principal component analysis
PDVF	Polyvinylidene difluoride
PKA	Protein kinase a
p-MLKL	Phosphorylated mixed-lineage kinase
p-NF-κB	Phospho-NF-kappaB
PPARα	Peroxisome proliferator-activated receptor alpha
p-PKA	Phospho-PKA
RIP3	Receptor-interacting protein kinase 3
ROS	Oxidative stress reactive oxygen species
SD	Sprague Dawley
SDS-PAGE	Sodium dodecyl sulfate polyacrylamide gel electrophoresis
TC	Total cholesterol
TG	Triglycerides
TGF-β	Transforming growth factor beta
TNF-α	Tumor necrosis factor alpha
TCM	Traditional Chinese medicine
UPLC-MS/MS	Ultra-performance liquid chromatography tandem mass spectrometry/mass spectrometry
XYS	Xiaoyao San

Nonalcoholic fatty liver disease (NAFLD) is a metabolic disorder characterized by excessive lipid accumulation in hepatocytes, independent of significant alcohol consumption. It is closely associated with obesity, dyslipidemia, and insulin resistance (IR), and has become the leading cause of chronic liver disease globally. The prevalence of NAFLD is rising in tandem with the increasing rates of obesity and diabetes, posing a significant burden on public health. By 2030, it is projected that the overall prevalence of NAFLD in adults will reach 33.5%[1]. Despite its significant impact, there is currently no approved pharmaceutical intervention for NAFLD, highlighting the urgent need for novel therapeutic strategies.

Traditional Chinese Medicine (TCM), a cornerstone of Chinese cultural heritage, is increasingly recognized as a complementary and alternative approach in modern medicine. TCM formulations, particularly those composed of multiple herbal components, are distinguished by their ability to facilitate synergistic interactions among diverse bioactive compounds. This multifaceted interaction profile endows TCM formulations with the potential to provide effective therapeutic interventions for a wide range of human diseases. Several TCM formulations, such as Yinchenhao Decoction, Shenling Baizhu Powder, Dachaihu Decoction, and Taohong Siwu Decoction, have shown significant efficacy in ameliorating the hepatic pathological manifestations of NAFLD[2]. However, the identification of specific ingredients and molecular targets within these formulations remains challenging. The burgeoning field of omics technology, particularly the application of transcriptomics and proteomics, has emerged as a valuable tool for diagnosing NAFLD[3]. Advances in understanding the pathophysiology of NAFLD[4] have facilitated the development of disease diagnosis and staging models, as well as the identification of potential therapeutic targets. To date, transcriptomics and proteomics have emerged as powerful tools for elucidating the biological changes associated with NAFLD and for understanding the multi-target therapeutic effects of drugs on this disease[5]. The integration of transcriptomics and proteomics provides a comprehensive depiction of the biological mechanisms in NAFLD tissues and cells. This combined approach is conducive to analyzing protein interactions, identifying highly expressed genes and pivotal regulatory elements, and screening for molecules and pathways with diagnostic and therapeutic potential. Consequently, the synergistic application of transcriptomics and proteomics can effectively elucidate the molecular mechanisms underlying the treatment of NAFLD with Chinese herbal medicine.

Xiaoyao San (XYS) is a traditional Chinese herbal formula originating from the *Taiping Huimin Heji Jufang*, composed of eight key medicinal herbs: *Bupleurum chinense* DC, *Angelica sinensis* (Oliv.) Diels, *Poria cocos* (Schw.) Wolf, *Paeonia lactiflora* Pall., *Atractylodes macrocephala Koidz*., *Glycyrrhiza uralensis* Fisch., *Mentha haplocalyx* Briq., and *Zingiber officinale* Rosc. These components, widely utilized in Asia, have a historical association with treating chronic liver diseases, such as liver fibrosis[6] and cirrhosis[7]. Recent pharmacological

studies have enlightened the diverse therapeutic effects of XYS, which include reducing hepatic steatosis[8], improving lipid and glucose metabolism, anti-inflammatory properties[9], demonstrating anti-oxidative stress capabilities[10], correcting intestinal flora imbalance[11], preventing hepatic fibrosis[12], and no obvious adverse drug reactions[13]. These findings indicate that XYS can significantly mitigate the pathological effects of NAFLD. However, the underlying mechanisms of XYS in treating NAFLD remain to be fully elucidated. In this study, we established a rat model of NAFLD to investigate the therapeutic effects of XYS through pathological and molecular biological analyses. We integrated pharmaceutical chemical analysis, transcriptomics, and proteomics to explore the chemical composition of XYS and its mechanism of action in NAFLD treatment. Our results provide a foundational understanding of the molecular mechanisms through which XYS addresses NAFLD.

Material

Animals

All experimental protocols and procedures adhered to the National Institutes of Health guidelines for the care and use of laboratory animals and were reviewed and approved by the Animal Ethics Committee of Xinjiang Medical University (Animal certificate No.: 65000700000940; Production license No.: SYXK-Xin-2023-0002). Every effort was made to minimize animal suffering and to use the minimum number of animals necessary to obtain reliable results. All procedures were performed in accordance with the ARRIVE guidelines. 24 male Sprague–Dawley (SD) rats, 6–8 weeks old and free of specific pathogens, weighing 180–220 g, were obtained from the Animal Centre of Xinjiang Medical University.

Experimental drugs

XYS was used in this study, with the following composition: *Bupleurum chinense* DC (30 g), *Angelica sinensis* (Oliv.) Diels (30 g), *Paeonia lactiflora* Pall. (30 g), *Atractylodes macrocephala* Koidz. (30 g), *Poria cocos* (Schw.) Wolf (30 g), *Mentha haplocalyx* Briq. (10 g), *Zingiber officinale* Rosc. (10 g), and *Glycyrrhiza uralensis* Fisch. (15 g). The crude drug decoction pieces were purchased from Beijing Tongrentang Decoction Co., Ltd. The preparation process strictly followed the "Chinese Pharmacopoeia" (2020 edition). The coarse powder of the medicinal materials was soaked in six times the volume of water for 1 h. The mixture was brought to a boil, then simmered at low heat for 2 h. The liquid was filtered, and the residue was boiled again with four times its volume of water for 2 h at low heat. The resulting liquid was filtered again. The two batches of medicinal liquid were combined and concentrated to a concentration of 1.927 g/mL in a water bath, then stored at 4 °C. Using a body weight conversion factor of 6.25, the adult daily dosage of the crude medicine was calculated to be 185 g. Based on the average adult body weight of 60 kg, the equivalent dosage for rats was determined to be 19.27 g/(kg•day). This dosage was administered continuously for 4 weeks, with a gavage volume of 1 mL/100 g body weight.

Reagents

High fat diet (HFD) (Beijing Boaigang Biotechnology Co., Ltd.); Ordinary experimental rat feed (Jiangsu Medicience Biomedical Co., Ltd.); H&E staining solution (Biosharp); Rat interleukin 1β (IL-1β), rat interleukin 6 (IL-6), rat tumor necrosis factor α (TNF-α), rat reactive oxygen species (ROS), rat cyclic adenosine monophosphate (cAMP)) ELISA kit (Shanghai Sinobest Biological Technology Co., Ltd.); Bovine serum albumin (Wuhan Chucheng Zhengmao Technology Engineering Co., Ltd.); Dithiothreitol, Trihydroxymethylaminomethane (Solarbio);Benzylmethylsulfonyl fluoride (Xiya Reagent); Tetraethylammonium bromide, urea (Sigma); BCA protein quantitative kit (Beyotime); Methanol, acetonitrile (Merck); Formic acid (Aladdin); Protein kinase A (PKA) antibody, phosphorylated PKA (p-PKA) antibody, nuclear factor-κB (NF-κB) antibody, phosphorylated NF-κB (p-NF-κB) antibody, forkhead box O1 (FOXO1) antibody (Santa); Peroxisome proliferator-activated receptor α (PPARα) antibody, transforming growth factor-β1 (TGF-β1) antibody, Receptor-interacting protein kinase 3 (RIP3) antibody, and phosphorylated mixed-line kinase domain-like protein (p-MLKL) antibody (Affinity).

Instruments

Sigma Desktop High Speed Freezing Centrifuge (Sartorius, Germany); Ultrasonic cell disruptor (Ningbo Scientz Biotechnology Co., Ltd.); Full-wavelength microplate reader (Thermo Fisher Scientific Co., Ltd.); Automatic biological analyzer (Shenzhen Mindray Biomedical Electronics Co., Ltd.); Biological microscope (Nikon Imaging Instruments Co., Ltd.); Vacuum freeze dryer (Jiaimu); Electrophoresis instrument and electrophoresis tank (Beijing Liuyi Instrument Factory); Mass spectrometer (Bruker); and pipette (Eppendorf).

Ethical review

This experimental protocol was approved by the Ethical Review Committee of Animal Experiments of Xinjiang Medical University, and the animal ethics approval number was IACUC-20230508-25.

Methods

Analysis of chemical constituents and blood components of XYS

Six SD male rats were randomly assigned to a blank group and an administration group. Rats in the administration group received intragastric administration of XYS at a dose of 19.27 g/kg/d, while those in the blank group received an equal volume of normal saline intragastrically for 7 consecutive days, once a day. One hour after the final gavage, blood was collected from the abdominal aorta of the rats, and the supernatant was centrifuged. The chemical constituents and blood components of XYS were analyzed qualitatively and quantitatively using ultra-high-performance liquid chromatography-tandem mass spectrometry (UPLC-MS/MS). Furthermore, the mass spectrometry data were processed using Analyst 1.6.3 software.

Establishment and grouping of models

Eighteen male SD rats were subjected to an adaptive feeding period for 1 week. The rats were housed in an environment maintained at a room temperature of 18–22 °C, relative humidity of 50–60%, and a light–dark cycle of 12/12 h. They had unrestricted access to drinking water and food. Fresh food and water were provided daily, and the bedding was changed every two days. Twelve rats were then randomly selected and fed a HFD for 10 weeks to induce a NAFLD rat model. The HFD composition included: 48.5% rat maintenance feed, 10% lard, 3% sesame oil, 2% cholesterol, 20% fructose, 12% casein, 2% mineral mixture, 2% calcium hydrogen phosphate, and 0.5% sodium cholate. These rats were further randomly divided into two groups: a NAFLD group and an XYS group. Rats in the XYS group received XYS at a dose of 19.27 g/kg/day by gavage, while those in the NAFLD group received an equal volume of normal saline by gavage for 4 weeks. The remaining six rats were assigned to the normal control (NC) group and were fed a standard diet. The body weight, food intake, and water intake of the rats were recorded weekly. In accordance with the 3R's principles (Reduction, Refinement, Replacement) of animal research and the absence of approved positive drug treatments for NAFLD, the establishment of a positive control group was omitted.

Specimen collection

Anesthesia was induced through the intraperitoneal injection of 2% pentobarbital at a dosage of 2 mL/kg. Blood samples were collected from the abdominal aorta, and centrifuged to obtain the supernatant. A section from the left lobe of the fresh liver tissue was fixed, and both frozen and paraffin sections of the liver tissue were prepared. Additionally, three liver tissues were placed in the freezing tubes, submerged in liquid nitrogen for rapid cooling for 1 h, and then transferred to a − 80 °C refrigerator for storage. Following specimen collection, rats were euthanized by carbon dioxide inhalation 5 min after anesthesia induction, in accordance with the AVMA Guidelines for the Euthanasia of Animals (2013).

Preparation and detection of liver transcriptomics samples

For ribonucleic acid (RNA) extraction, liver tissues from each group were processed using the Trizol method. The successfully extracted RNA was enriched with polyA tail mRNA by Oligo (dT) magnetic beads. Subsequently, a fragmentation buffer was introduced to break the RNA into short fragments. First-strand cDNA was synthesized using the fragmented RNA as a template and random hexamer primers. Then, double-stranded cDNA was synthesized by adding a buffer, dNTPs (dTTP, dATP, dGTP, dCTP), and DNA polymerase I. The double-stranded cDNA was purified using DNA purification magnetic beads, followed by end repair, A tail addition, and ligation of the sequencing adapter. The fragment size was selected with DNA purification magnetic beads, and the final cDNA library was constructed through PCR enrichment. After successful library construction and quality testing, the libraries were pooled according to the target data volume and sequenced on the Illumina platform by Metware Biotechnology Co., Ltd. (Wuhan, China).

Preparation and detection of liver proteomics samples

The liver tissues from each group were ground, lysed, and centrifuged to collect the supernatant for protein extraction. After that, the proteins were reduced with 10 mM DTT at 37 °C for 45 min and alkylated with 50 mM iodoacetamide in the dark at room temperature for 15 min. Subsequently, precooled acetone (four times the volume of the protein solution) was added, and the mixture was precipitated at − 20 °C for 2 h.

After centrifugation, the protein precipitate was dried and resuspended in a 200 μL solution containing 25 mM ammonium bicarbonate and 3 μL trypsin, followed by overnight digestion at 37 °C. The resulting peptides were desalted using a C18 column, concentrated by vacuum centrifugation, and re-dissolved in a 0.1% (v/v) formic acid solution. The prepared samples were detected by NanoElute high-performance liquid chromatography coupled with a timsTOF Pro2 mass spectrometer.

Observation indicators and methods

Histopathological observation of liver

The morphological changes in the livers of each group were visually inspected. Paraffin sections of rat liver tissue were prepared and stained with hematoxylin and eosin (H&E). The histopathological changes were assessed using the Nonalcoholic Fatty Liver Disease Activity Score (NAS). Additionally, liver tissues were frozen, sectioned, and stained with Oil Red O to observe pathology and lipid deposition under an optical microscope. The area ratio of lipid droplets in Oil Red O-stained sections was analyzed using Image-Pro Plus 6.0 software.

Detection of serum liver function, blood lipid, blood glucose, inflammatory factors, and ROS

Serum levels of liver function indicators, including alanine aminotransferase (ALT), aspartate aminotransferase (AST), and gamma-glutamyl transferase (GGT), were measured using an automatic biochemical analyzer. Lipid profile indicators, such as triglycerides (TG), total cholesterol (TC), high-density lipoprotein cholesterol (HDL-C), low-density lipoprotein cholesterol (LDL-C), and fasting blood glucose (FBG), were also assessed. Additionally, serum levels of inflammatory cytokines IL-1β, IL-6, TNF-α, and ROS were quantified using ELISA kits according to the manufacturer's instructions.

Validation of key proteins

The concentration of cAMP in liver tissue was determined by ELISA kits. Western blotting was employed to verify the key proteins. Liver tissues were lysed and centrifuged to obtain the supernatant. The protein concentration was detected using the bicinchoninic acid (BCA) assay. Equal amounts of protein (50 μg) were separated by sodium dodecyl sulfate polyacrylamide gel electrophoresis (SDS-PAGE) and transferred to a polyvinylidene difluoride (PVDF) membrane. The membrane was blocked with 5% skim milk for 90 min, and then incubated

with specific primary and secondary antibodies. After washing three times with tris-buffered saline with Tween 20 (TBST), the membrane was treated with freshly prepared ECL substrate for chemiluminescent detection. Later, protein band intensity was quantified via ImageJ software.

Data processing and statistical methods

The differentially expressed proteins or genes were identified and thoroughly analyzed through functional annotation. The criteria for selection included an absolute value of *log2Fold* Change ≥ 1 and a *False Discovery Rate (FDR)* < 0.05 or a *P*-value < 0.05. Only genes with statistically significant differential expression were included in subsequent enrichment analyses. Gene Ontology (GO) classification, Kyoto Encyclopedia of Genes and Genomes (KEGG) pathway analysis, and protein domain enrichment analysis were conducted for the differential genes or proteins in each group. The significance *P*-value for enrichment was calculated using the hypergeometric method. Statistical analysis was performed using SPSS 25.0 software, with measurement data presented as mean ± standard deviation (MEAN ± SD). *One-way ANOVA* was used to compare differences between groups. For cases of equal variance, the Least Significant Difference (*LSD*) method was adopted for multiple comparisons; otherwise, the Tamhane's *T2* method was applied. GraphPad Prism 9.5.1 was applied for plotting. A *P*-value < 0.05 was considered statistically significant.

Results

Chemical constituents and blood components of XYS

UPLC-Q-TOF-MS/MS technology was employed to analyze the chemical constituents of XYS and drug-containing serum. The total ion current diagram is shown in Fig. 1. The analysis identified a total of 2,174 components in XYS, including 398 flavonoids, 360 phenolic acids, 229 amino acids and derivatives, 185 terpenoids, 182 lipids, 154 alkaloids, 136 organic acids, 110 lignans and coumarins, 70 nucleotides and derivatives, 31 quinones, 30 tannins, and 289 other compounds. Further analysis of serum from rats administered XYS identified 259 blood components, including 91 alkaloids, 47 phenolic acids, 40 terpenoids, 28 flavonoids, 5 quinones, 5 lignans and coumarins, 1 tannin, and 42 other compounds. Specifically, 225 prototype chemical components of XYS were detected in the serum after administration, including 26 flavonoids, 39 terpenoids, 5 lignans and coumarins, 69 alkaloids, 44 phenolic acids, 4 quinones, 1 tannin, and 37 other compounds. (Supplementary Material 1).

Effect of XYS on NAFLD model rats in general conditions

The liver, a crucial organ in fat metabolism, accumulates excessive lipids following long-term HFD intake due to the combined effects of circulating free fatty acids (FFA), de novo lipogenesis, and dietary fat absorption, leading to obesity. Obesity, closely linked to NAFLD, can be assessed by monitoring body weight, liver index, and Lee's index in the NAFLD rat model. In establishing the HFD-induced NAFLD model, rats exhibited significant increases in food and water intake, body weight, liver index, and Lee's index, confirming obesity development (Fig. 2A–F). Post-XYS administration, food and water intake decreased significantly, and the elevated body weight, liver index, and Lee's index were reversed. These findings are illustrated in Fig. 2A–F.

Effects of XYS on the pathological changes in liver tissues in an NAFLD rat model

Liver lipid accumulation and inflammation are key markers of NAFLD[14]. The morphological and histological changes in rat livers were subjected to a comprehensive visual analysis, including direct visual inspection and detailed examination through H&E, and Oil Red O staining (Fig. 3A–C). Rats on HFD exhibited pale-yellow liver surface, greasy sections (Fig. 3A), swollen volumes, extensive hepatic steatosis, and significant lipid droplet accumulation with inflammatory cell infiltration (Fig. 3B and C). Dysregulation of liver lipid metabolism is closely associated with NAFLD onset and progression[15]. Meanwhile, NAFLD rats had higher NAS scores and Oil Red O area ratios, indicating greater pathological activity and lipid accumulation (Figs. 3D and 6E). Following XYS administration, liver tissue color normalized to dark red (Fig. 3A), lipid droplet distribution decreased, inflammatory cell infiltration reduced (Fig. 3B and C), and both NAS scores and Oil Red O area ratios were lower (Figs. 3D and 6E). These findings suggest that XYS significantly mitigates HFD-induced liver lipid accumulation and ameliorates liver inflammation.

Effects of XYS on serum liver function, glucose and lipid metabolism, and inflammatory factors in an NAFLD rat model

The elevated levels of serum transaminases (ALT, AST, and GGT) are indicative of hepatocellular injury and serve as reliable biomarkers for assessing the severity of fatty liver disease (FL)[16]. Lipid accumulation-induced hepatocellular injury results in the release of these enzymes into the bloodstream. As shown in Fig. 4A–C, NAFLD rats models fed a HFD exhibited significantly increased levels of ALT, AST, and GGT, reflecting liver injury. But after administration of XYS, the liver injury was mitigated, as evidenced by the normalization of ALT, AST, and GGT levels.

HFD-induced disruption of lipid metabolism leads to significant hepatic lipid accumulation, resulting in steatosis, which is closely associated with IR[17]. The liver, a central metabolic organ, plays a crucial role in regulating and monitoring serum lipid and glucose levels. But, it was observed (Fig. 4D–G) that long-term HFD consumption led to elevated serum levels of TC, TG, and LDL-C, while reducing HDL-C levels. In contrast, XYS administration alleviated these metabolic disturbances. HFD-induced IR increases glucose production and causes blood glucose fluctuations, leading to elevatedFBG levels in NAFLD rats. In contrast, XYS intervention normalized FBG levels and corrected glucose metabolism disorders (Fig. 4H). Additionally, long-term HFD consumption promotes lipid accumulation and increases lipid peroxidation, rendering lipids more susceptible to oxidative damage by ROS, ultimately leading to liver. This oxidative stress, in turn, also triggers an inflammatory response that exacerbates the progression of NAFLD[18]. In this study, serum levels of inflammatory cytokines (IL-

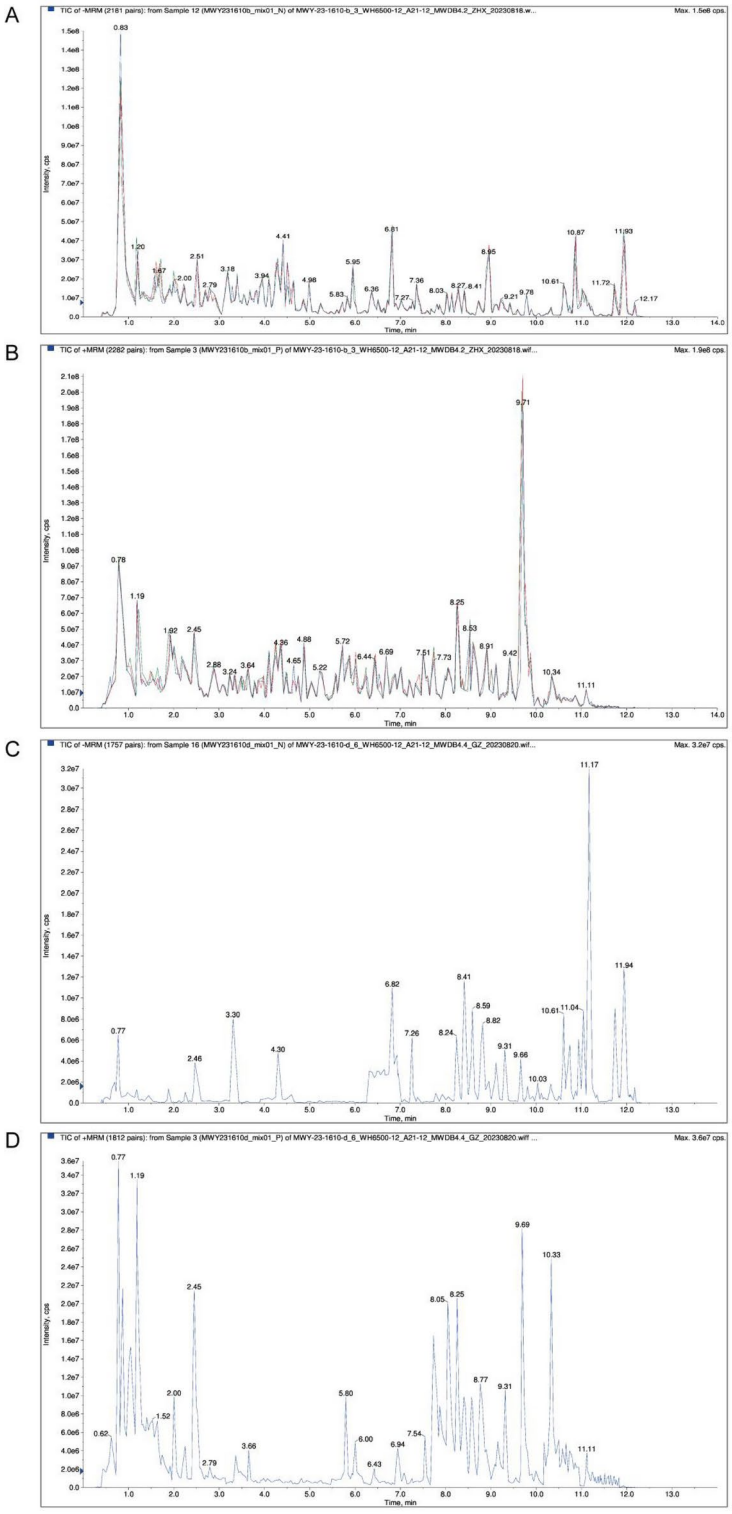

Fig. 1. Total ion current diagrams of XYS mass spectrometry analysis in (**A**) negative ion mode, and (**B**) positive ion mode, and of XYS drug-containing serum in (**C**) negative ion mode, and (**D**) positive ion mode.

1β, IL-6, TNF-α) and ROS injury (Fig. 4I–L) were elevated in NAFLD rats, but XYS administration significantly reduced these levels, thereby attenuating both inflammation and oxidative stress.

Effects of XYS on liver transcriptomics in an NAFLD rat model

To investigate the changes in gene expression, transcriptome analysis was performed on the livers of NAFLD model rats treated with XYS. Principal component analysis (PCA) revealed significant differences in the

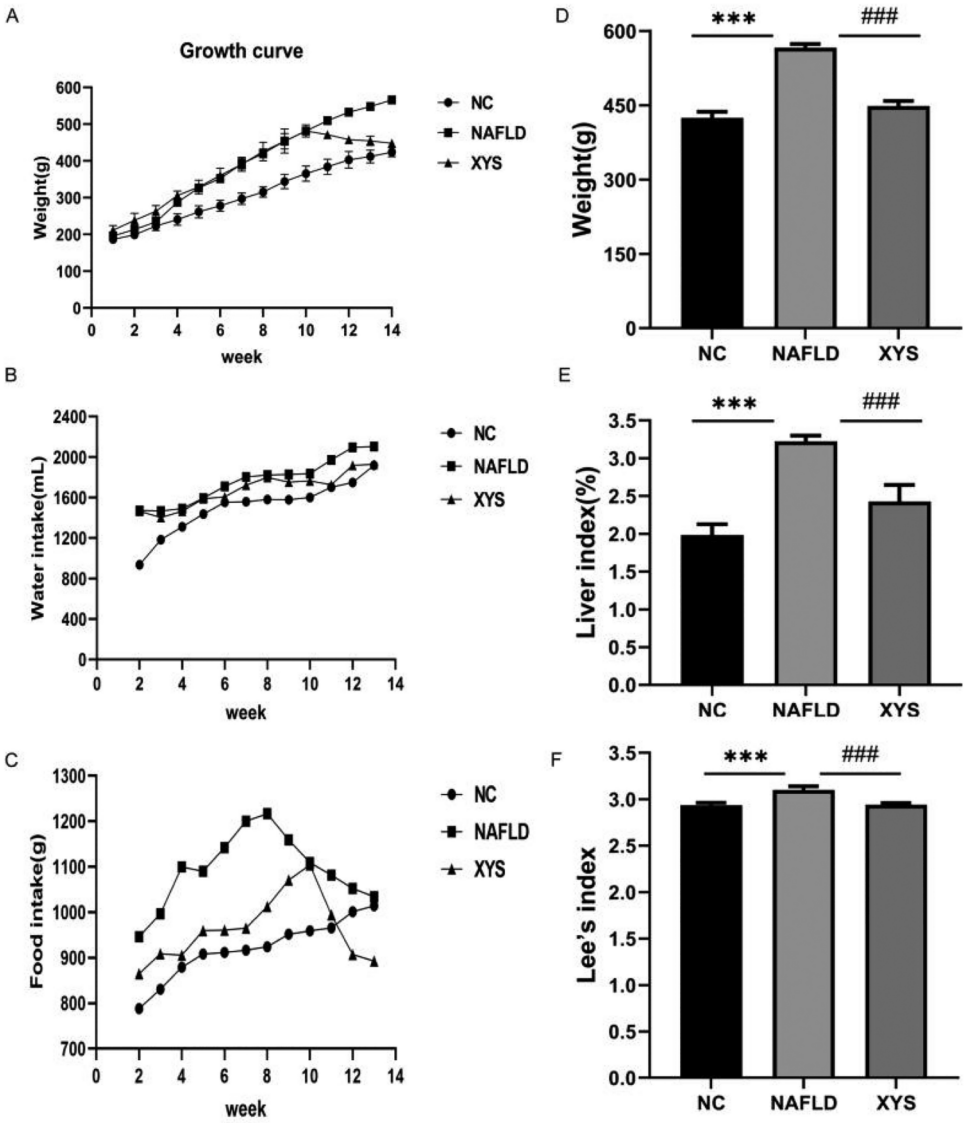

Fig. 2. Growth curves (**A**), water intake (**B**), food intake (**C**), body weight (**D**), liver index (**E**), and Lee's index (**F**) of rats in different groups. $^{*}P<0.05$, $^{**}P<0.01$, $^{***}P<0.001$, vs NC group; $\#P<0.05$, $\#\#P<0.01$, $\#\#\#P<0.001$, vs NAFLD group.

transcriptome between the NC group and the NAFLD group, with minimal differences between the XYS-treated group and the NC group (Fig. 5A). This suggests that XYS treatment mitigates transcriptional alterations associated with NAFLD. Volcano plots (Fig. 5C and D) identified 227 differentially expressed genes (DEGs) between the NC and NAFLD groups, and 793 DEGs between the NAFLD and XYS groups. In between the NC and NAFLD groups, 88 genes were upregulated, while 139 genes were downregulated. In contrast, between NAFLD and XYS groups data revealed that 388 genes were upregulated and 404 genes were downregulated in the XYS-treated rats (Fig. 5B). Heatmaps (Fig. 5E) illustrated the gene expression patterns between the NC and NAFLD groups, and between the NAFLD and XYS groups.

Effects of XYS on liver proteomics in an NAFLD rat model

PCA was performed to assess the overall differences in protein expression and the degree of variation within and between groups. As illustrated in Fig. 6A, significant differences in protein profiles were observed between rats fed HFD and those treated with XYS, indicating that XYS effectively mitigated HFD-induced proteomic changes. Volcano plots (Fig. 6C and D) identified 298 DEPs between the NC and NAFLD groups, and 252 DEPs between the NAFLD and XYS groups. In the NC and NAFLD groups, 164 proteins were upregulated and 134 were downregulated, respectively. In contrast, XYS treatment resulted in the upregulation of 119 proteins and downregulation of 133 proteins in NAFLD rats (Fig. 6B). Heatmaps (Fig. 6E) demonstrated the protein expression patterns between the NC and NAFLD groups, and between the NAFLD and XYS groups, respectively.

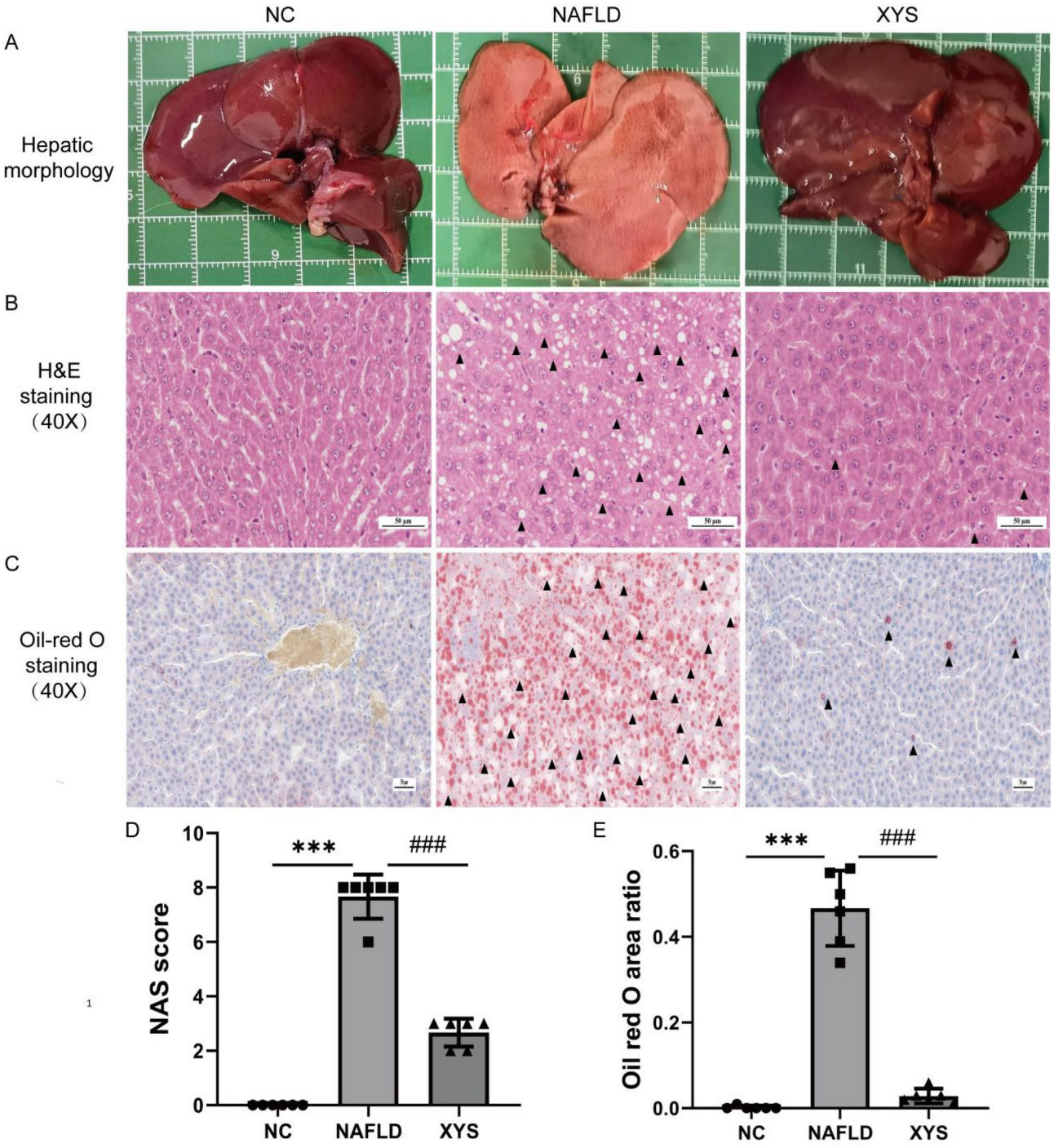

Fig. 3. Morphological changes of liver in each group (**A**); H&E staining results on pathological changes in liver (**B**); Lipid accumulation in the liver observed by Oil red O staining (**C**). ▲: Lipid droplet distribution. NAS score (**D**), and Oil red O area ratio (**E**) in each group. $^{*}P<0.05$, $^{**}P<0.01$, $^{***}P<0.001$, vs NC group; $\#P<0.05$, $\#\#P<0.01$, $\#\#\#P<0.001$, vs NAFLD group.

The effect of XYS on the combined analysis of liver transcriptomics and proteomics in an NAFLD rat model

The complex and holistic nature of NAFLD necessitates a multi-omics approach to elucidate its regulatory mechanisms and identify key metabolic pathways, proteins, and genes. Integrating transcriptomics and proteomics data reduces the likelihood of false positives associated with single-omics analyses, facilitating deeper exploration of NAFLD's regulatory mechanisms. The mRNA data from transcriptomics were matched and integrated with protein data from proteomics. Venn analysis identified 11 (including Plcb1, Stac3, Dipk2a, Eci1, Ces2a, Elovl2, Amacr, Hacl1, Cyp17a1, Ech1, and Siglec1), and 14 (including Atp1b1, Pcsk9, Crot, Plin2, Cyp51,

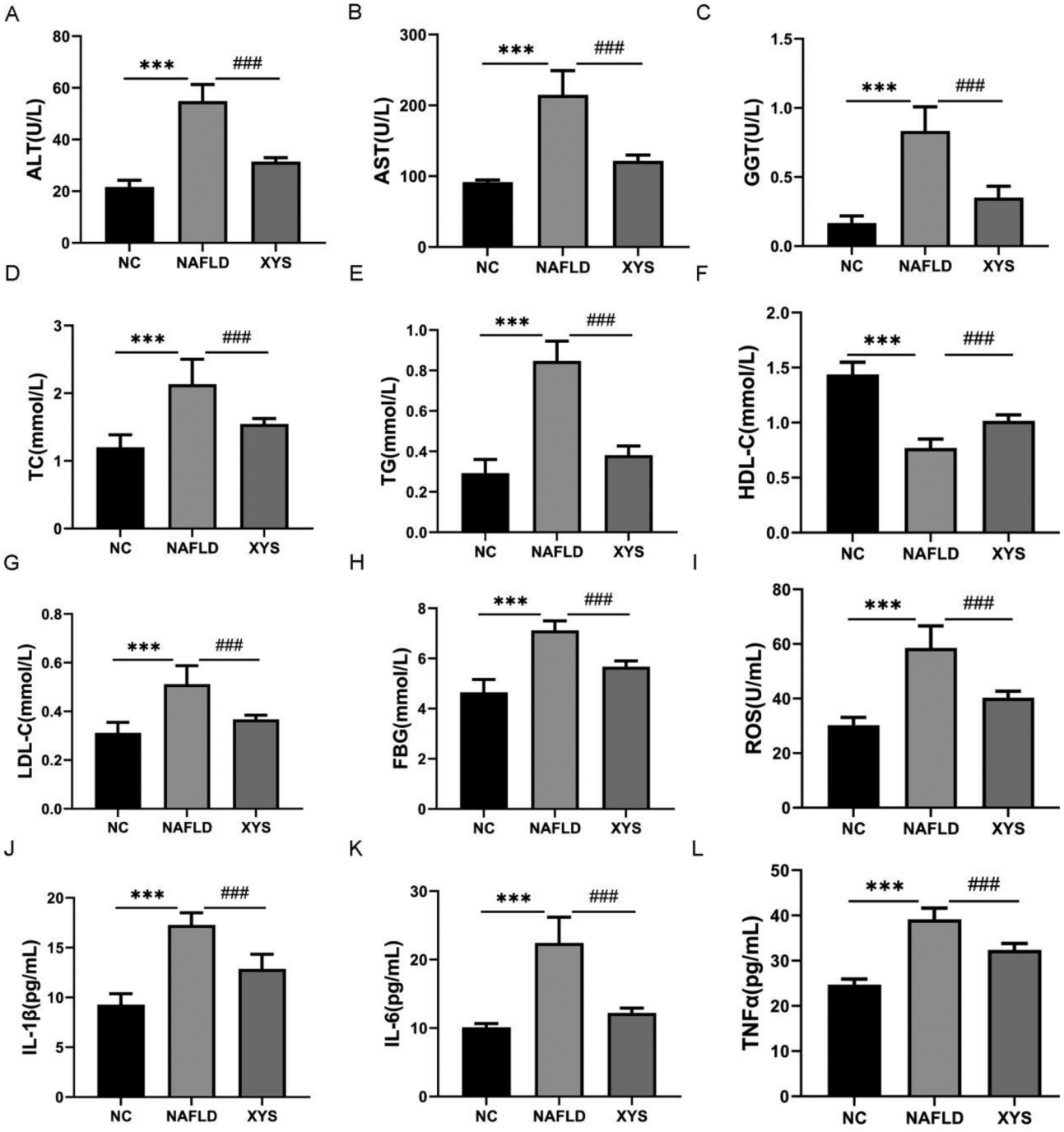

Fig. 4. The levels of ALT (**A**), AST (**B**), GGT (**C**), TC (**D**), TG (**E**), HDL-C (**F**), LDL-C (**G**), FBG (**H**), ROS (**I**), IL-1β (**J**), IL-6 (**K**), and TNF-α (**L**) in serum of rats in each group. $^{*}P<0.05$, $^{**}P<0.01$, $^{***}P<0.001$, vs NC group; $\#P<0.05$, $\#\#P<0.01$, $\#\#\#P<0.001$, vs NAFLD group.

A2ml1, Acat1, Slc13a2, Bhmt, Pkia, Fads1, Dhcr7, Tm7sf2, and Ido2) DEGs and DEPs between the NC and NAFLD groups as well as the NAFLD and XYS groups, respectively (Fig. 7A and B). The comparative analyses of differential expression levels and fold changes were visualized using heatmaps and scatter plots (Fig. 7C and D). The GO enrichment analysis deferentially expressed genes or proteins between the transcriptome and proteome highlighted the top 10 entries (Fig. 7E and F). The multi-omics results between the NC group and the NAFLD group indicated that NAFLD primarily involved biological processes (BP), including fatty acid and triglyceride metabolism, fatty acid oxidation, biosynthesis of unsaturated fatty acids, precursor metabolites, and energy production. The cellular components (CC) included peroxisomes, vacuole membranes, and endoplasmic reticulum components. Molecular composition (MF) were associated with iron ion binding, acyltransferase activity, carboxylesterase activity, and oxidoreductase activity. To investigate the representative signaling

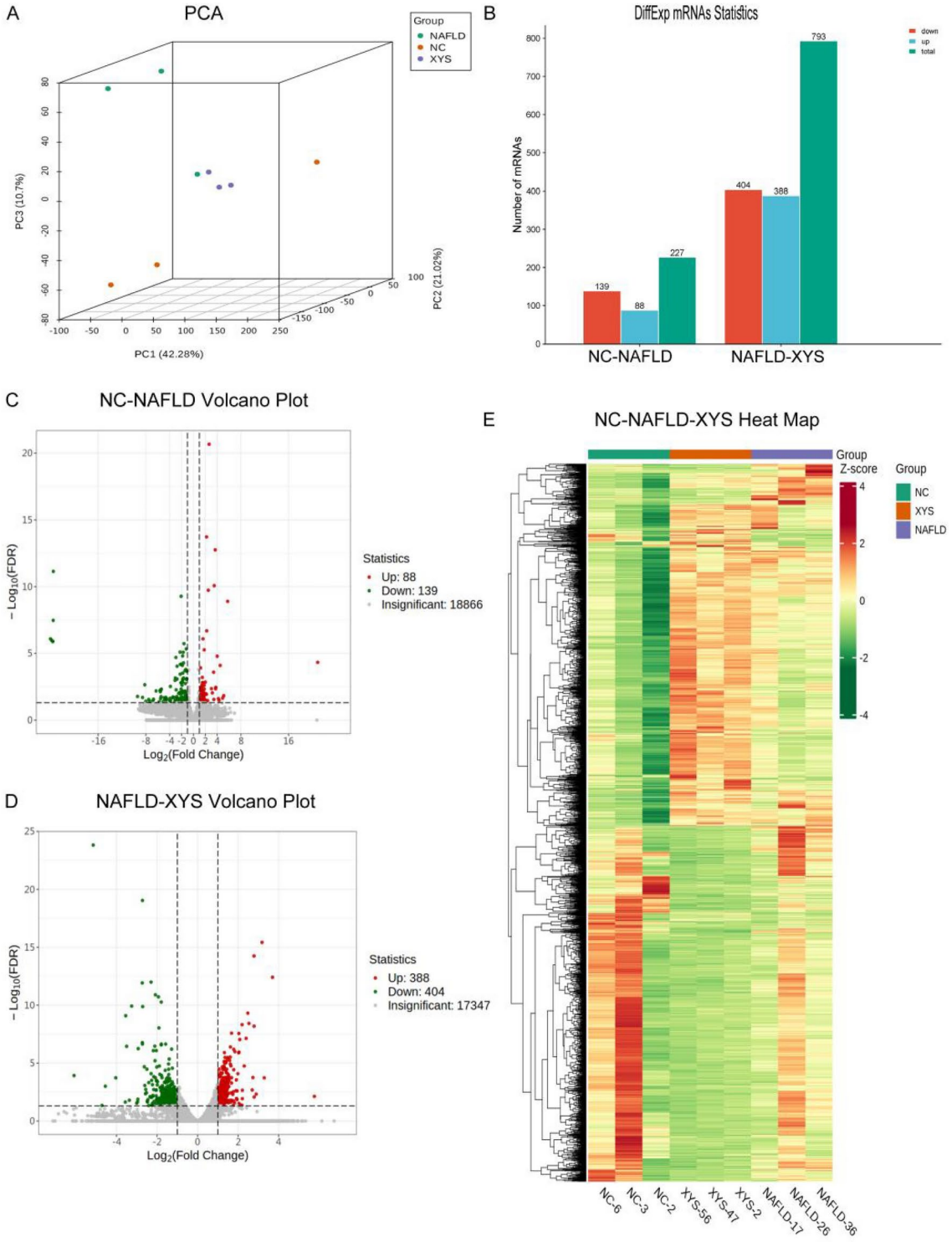

Fig. 5. Analysis of the difference of mRNA expression level in liver tissue between NC group or XYS group and NAFLD group. (**A**): PCA results of RNA-seq data. (**B**): Histogram of differential gene expression among different groups. (**C**, **D**): Volcano maps depicting the relative abundance of transcripts. The abscissa represented the change of gene expression multiples, and the ordinate marked the significance level of differential genes. The red and green dots indicated the up-regulated and downregulated differential genes, respectively; and the gray dots referred to non-DEGs. (**E**): Heat maps of gene expression among different groups. The abscissa represented the sample name and hierarchical clustering results, and the ordinate was the differential genes and hierarchical clustering results. Red indicated high expression while blue signified low expression.

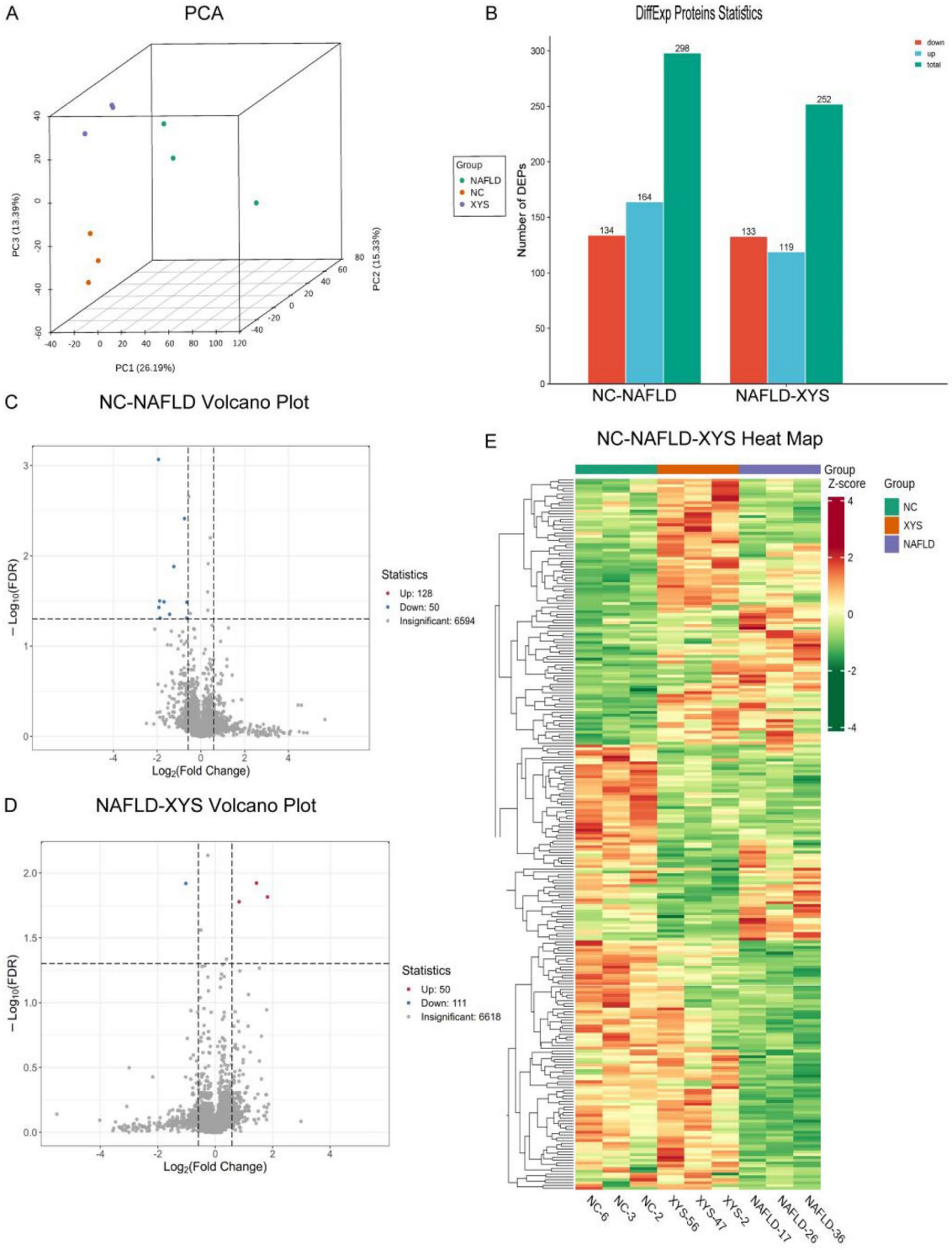

Fig. 6. Difference analysis of protein expression levels in liver tissues between NC group or XYS group and NAFLD group. (**A**): PCA results of proteome data. (**B**): Histogram of differential protein expression. (**C**, **D**): Volcanic maps displaying the relative abundance of proteins. The abscissa represented the change of protein expression multiples, and the ordinate showed the significance level of differential proteins. The red and green dots marked the upregulated and downregulated DEPs, respectively, and the gray ones were non-DEPs. (**E**): Heat maps for protein expression. The abscissa represented the sample name and hierarchical clustering results, and the ordinate signified the differential protein and hierarchical clustering results, with red and green indicating high and low expression, respectively.

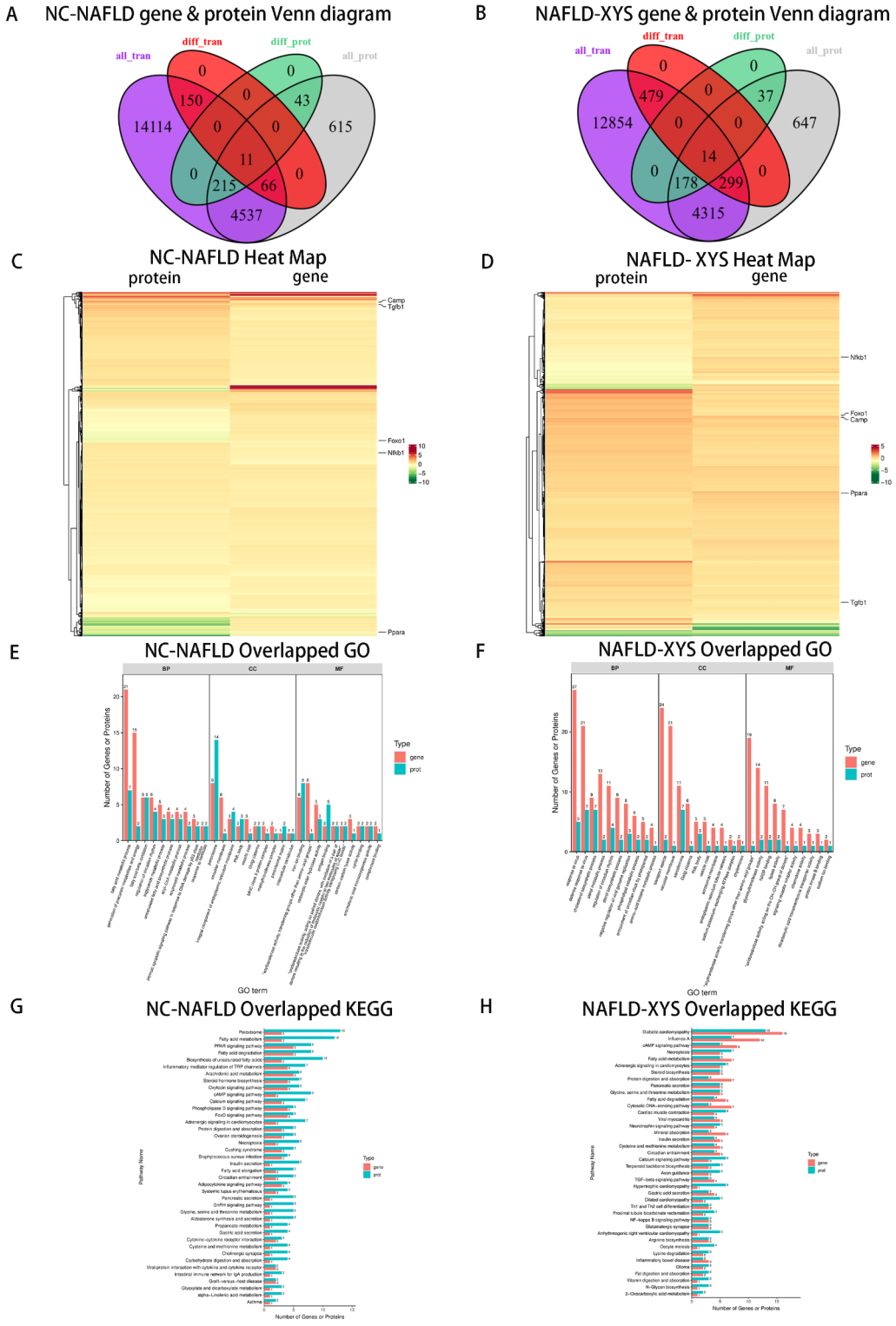

pathways associated with key targets in the NC and NAFLD groups, KEGG enrichment analysis was conducted. The analysis revealed pathways related to peroxisomal function, fatty acid and carbohydrate metabolism, protein processing, and insulin signaling. Additionally, several critical signaling pathways were identified, including PPARα, cAMP, FOXO, and necroptosis (Fig. 7G and H). GO analysis between the NAFLD and XYS groups identified significant BP associated with cholesterol, sterol, phospholipid, and amino acid betaine metabolism. CC implicated included transport vesicles, vacuolar membranes, Golgi apparatus, PML body vesicles, and endoplasmic reticulum. MF were predominantly related to acyltransferase activity, glycosyltransferase activity, NADP binding, lipase activity, oxidoreductase activity, and others.

Between the NAFLD group and the XYS group, the KEGG enrichment analysis highlighted key signaling pathways associated with fatty acid metabolism, protein metabolism, insulin signaling, gastric acid metabolism, and critical pathways such as cAMP, TGF-β, NF-κB, FOXO, and necroptosis (Fig. 7E and F).

Fig. 7. Venny diagram of DEPs and DEGs between the NC group and the NAFLD group (**A**) and that between the NAFLD group and the XYS group (**B**). Note: all_tran and diff_tran represented all genes and DEGs identified by the transcriptome, respectively; all_prot and diff_prot signified all proteins and DEPs identified by the proteome, respectively. Protein and gene differential fold clustering heat map between the NC group and the NAFLD group (**C**) and that between the NAFLD group and the XYS group (**D**). Note: Each row in the figure represented a protein or a corresponding gene, and the two columns were the difference multiples of the proteome and transcriptome data, respectively. The red part marked the up-regulated protein or gene, while the downregulated protein or gene was labelled in green. GO enrichment analysis results of DEGs and DEPs in each group based on transcriptome and proteome (**E**, **F**). Note: The abscissa represented the secondary GO item, and the ordinate represented the number of genes or proteins enriched to the GO item. Bar charts based on the results of KEGG pathway enrichment analysis (**G**, **H**). Note: The abscissa represented the number of differential proteins and differential genes enriched in the pathway, the ordinate represented the KEGG pathway name, and the red and green bars represent the transcriptome and proteome, respectively.

Screening of key proteins and experimental verification

To validate the results from transcriptomics and proteomics analyses and to predict the core mechanism of XYS in treating NAFLD, we screened and verified the expression of key proteins, including cAMP, PKA, PPARα, FOXO1, NF-κB, RIP3, p-MLKL and TGF-β1 (Fig. 8A–I), in liver tissues. ELISA results indicated that HFD-induced reduction in hepatic cAMP levels was significantly restored following XYS administration. Western blotting revealed that long-term HFD downregulated the expressions of PKA, p-PKA, and PPARα, while upregulating the expressions of NF-κB, p-NF-κB, FOXO1, TGF-β1, RIP3, and p-MLKL. In contrast, XYS treatment restored the expressions of PKA, p-PKA, and PPARα, while concurrently decreasing the expressions of NF-κB, p-NF-κB, FOXO1, TGF-β1, RIP3, and p-MLKL. The schematic key molecular pathways implicated in NAFLD development and XYS intervention are highlighted in Fig. 9, which also depicts the suggested mechanism of XYS in NAFLD therapy (generated from integrated transcriptomic and proteomic studies utilizing KEGG pathway data).

Discussion

NAFLD stands as the second most prevalent chronic liver disease worldwide[20], potentially progressing to nonalcoholic steatohepatitis (NASH), cirrhosis, and hepatocellular carcinoma (HCC), posing a serious threat to public health. A global call to action[21] emphasized the need for countries to collaboratively develop and implement a comprehensive and long-term NAFLD public health agenda. Excessive free fatty acids (FFA) are recognized as a crucial initiating factor in NAFLD[22], disrupting lipid metabolism and inducing oxidative stress, inflammation, and IR[17], even liver cell damage and death[23,24]. This imbalance contributes to NAFLD progression, as observed in HFD-induced animal models[25]. Long-term HFD intake leads to steatosis, IR, necroptosis, and liver fibrosis[26]. Due to complex pathogenesis of NAFLD, effective treatment strategies are urgently needed.

Chinese herbal medicine, a vast repository of medical knowledge, presents unique advantages in the treatment of various liver diseases[27] due to its efficacy, and minimal side effects. The XYS, a classical Chinese prescription, is widely used in the treatment of gastrointestinal disorders, particularly NAFLD. A meta-analysis[28] demonstrated that XYS can regulate blood lipids, protect liver function, and prevent the NAFLD progression. To further clarify the chemical composition and bioavailable components of XYS, UPLC-MS/MS analysis was performed. This approach identified 2174 compounds in XYS, including 225 prototype chemical constituents retained in the bloodstream after administration. In view of the multi-component and multi-target nature of Chinese herbal medicines, high-throughput techniques such as transcriptomics and proteomics are essential for identifying drug targets and elucidating their mechanisms of action. In this research, the integration of transcriptomics and proteomics revealed that XYS treatment primarily involves fatty acid metabolism, insulin metabolism, and key signaling pathways such as cAMP, TGF-β, NF-κB, and necroptosis. It is well established that the liver plays a central role in fat metabolism, including processing and storage, with lipolysis initiated by cAMP/PKA signaling[29]. The cAMP/PKA pathway is crucial in regulating lipid metabolism and is closely associated with NAFLD progression[30]. Decreased PKA activity is linked to TG accumulation in the liver, a significant factor in NAFLD progression[31]. PKA is composed of two regulatory subunits and two catalytic subunits, and its activity is influenced by cAMP. The elevated intracellular cAMP levels promote its binding to the regulatory subunit of PKA, leading to the release of the active catalytic subunit and subsequent PKA activation[24,31]. Activated PKA-C phosphorylates downstream substrates, suppresses the transcriptional activity of target genes involved in lipid metabolism, reduces the expression of fat-associated genes[32], and enhances lipolysis[33], thereby reducing hepatic lipid accumulation. Additionally, studies have demonstrated that PKA phosphorylation can regulate PPARα activity[34]. PPARα is predominantly expressed in the liver[35], serves as a main driving force for metabolic regulation, is an essential transcription factor for regulating lipid and glucose homeostasis[36], and high fatty acid oxidation. PPARα expression is inversely correlated with NAFLD presence and steatosis severity[37]. Overexpression or activation of PPARα mitigates oxidative stress, reduces lipid deposition, improves IR[38], and corrects metabolic disorders. PPARα agonists demonstrate anti-adipogenic effects[39], and Chinese herbal compound[40] or monomer[41] can elevate PPARα expression, decreases oxidative stress, and hepatic steatosis. Furthermore, PPARα regulation activates the downstream transcription factor FOXO1, inhibiting TG synthesis[42], and delaying NAFLD progression. PKA plays a pivotal role in mediating the effects of FOXO1 and is involved in liver lipid metabolism and glucose homeostasis[43–45]. Over the past decade, FOXO1 has emerged as a transcriptional regulator influencing multiple genes involved in regulation of autophagy, inflammation, adipogenesis, oxidative stress, and necroptosis, thus affecting liver metabolism[46–49]. Furthermore, FOXO1 promotes liver fibrosis through TGF-β1-mediated activation of hepatic stellate cells[50]. Consequently,

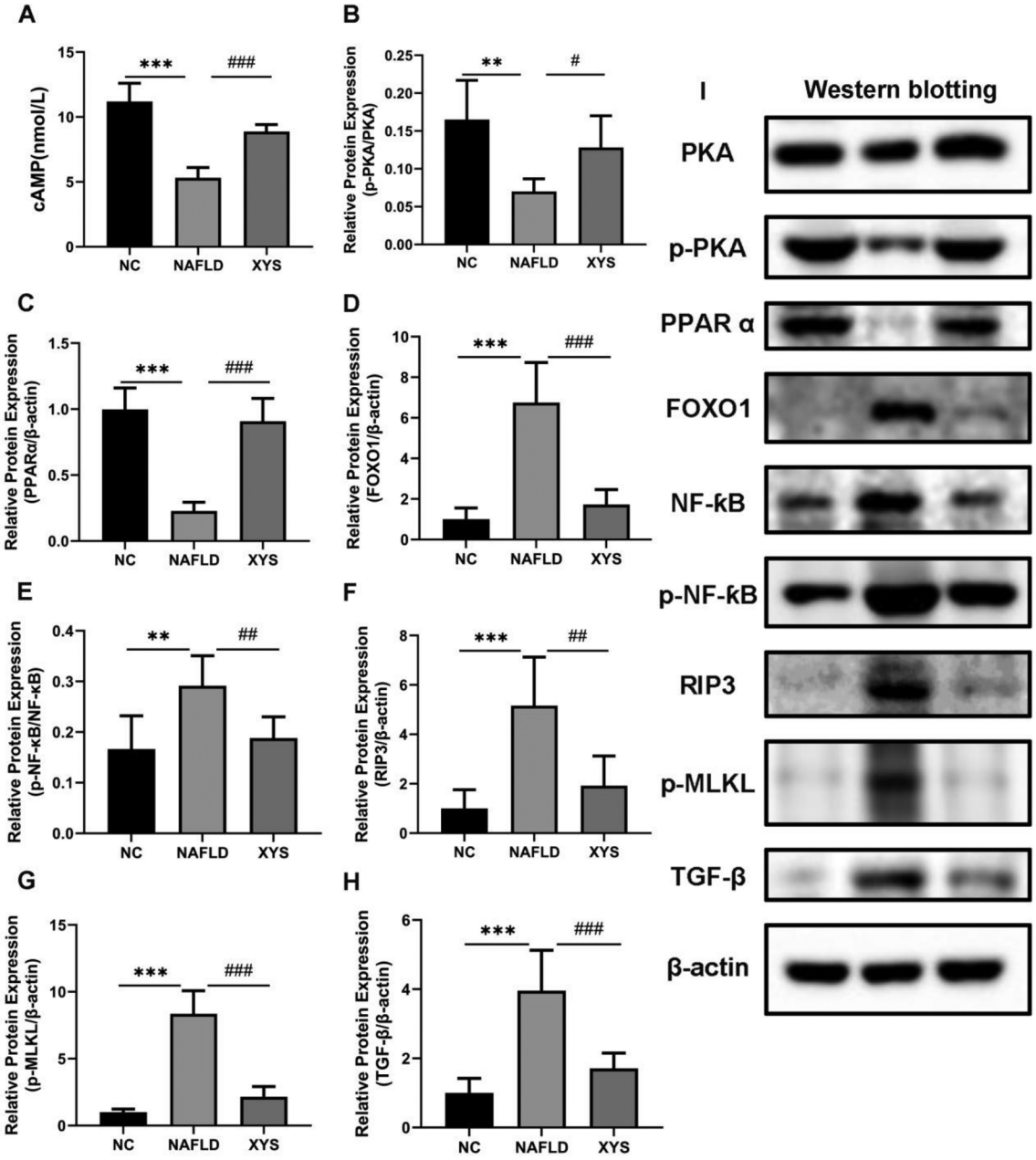

Fig. 8. ELISA results of cAMP content (**A**) in liver tissue of rats in each group. Quantitative analysis of p-PKA/PKA (**B**), PPARα (**C**), FOXO1 (**D**), p-NF-κB/NF-κB (**E**), RI3P (**F**), p-MLKL (**G**) and TGF-β (**H**) protein in liver tissue of rats in each group. $^{*}P<0.05$, $^{**}P<0.01$, $^{***}P<0.001$, vs NC group; $\#P<0.05$, $\#\#P<0.01$, $\#\#\#P<0.001$, vs NAFLD group.

FOXO1 is considered a potential therapeutic target for both NAFLD[48] and liver fibrosis[50]. In addition, PKA attenuates the transcriptional activity of NF-κB[51], and suppresses the expression of inflammatory factors. NF-κB, a heterodimeric protein composed of p65 and p50 subunits, exhibits transcriptional activity primarily through the p65 subunit[52,53]. Activation of the NF-κB signaling pathway results in the phosphorylation and nuclear translocation of p65, thereby enhancing inflammation and lipid deposition while downregulating the expression of inflammatory genes in hepatocytes[54]. Studies have demonstrated that herbal extracts inhibit the expression of NF-κB and downregulate the expression of downstream inflammatory cytokines, including TNFα, IL-6, IL-1β, and TGF-β1, by modulating the NF-κB signaling pathway in NAFLD rats[55–57]. TGF-β1, a potent mediator of liver fibrosis, promotes fibrotic processes when overexpressed in hepatocytes. Consequently, inhibiting NF-κB signaling and reducing TGF-β1 levels can mitigate liver inflammation and prevent the progression of liver fibrosis. Thus, the NF-κB signaling pathway is crucial in the progression of oxidative stress, inflammation, and fibrosis in NAFLD[57,58]. Moreover, both in vivo and in vitro studies have demonstrated that regulation of the NF-κB pathway significantly reduces necrotic apoptosis of hepatocytes[59], and ameliorates oxidative stress and

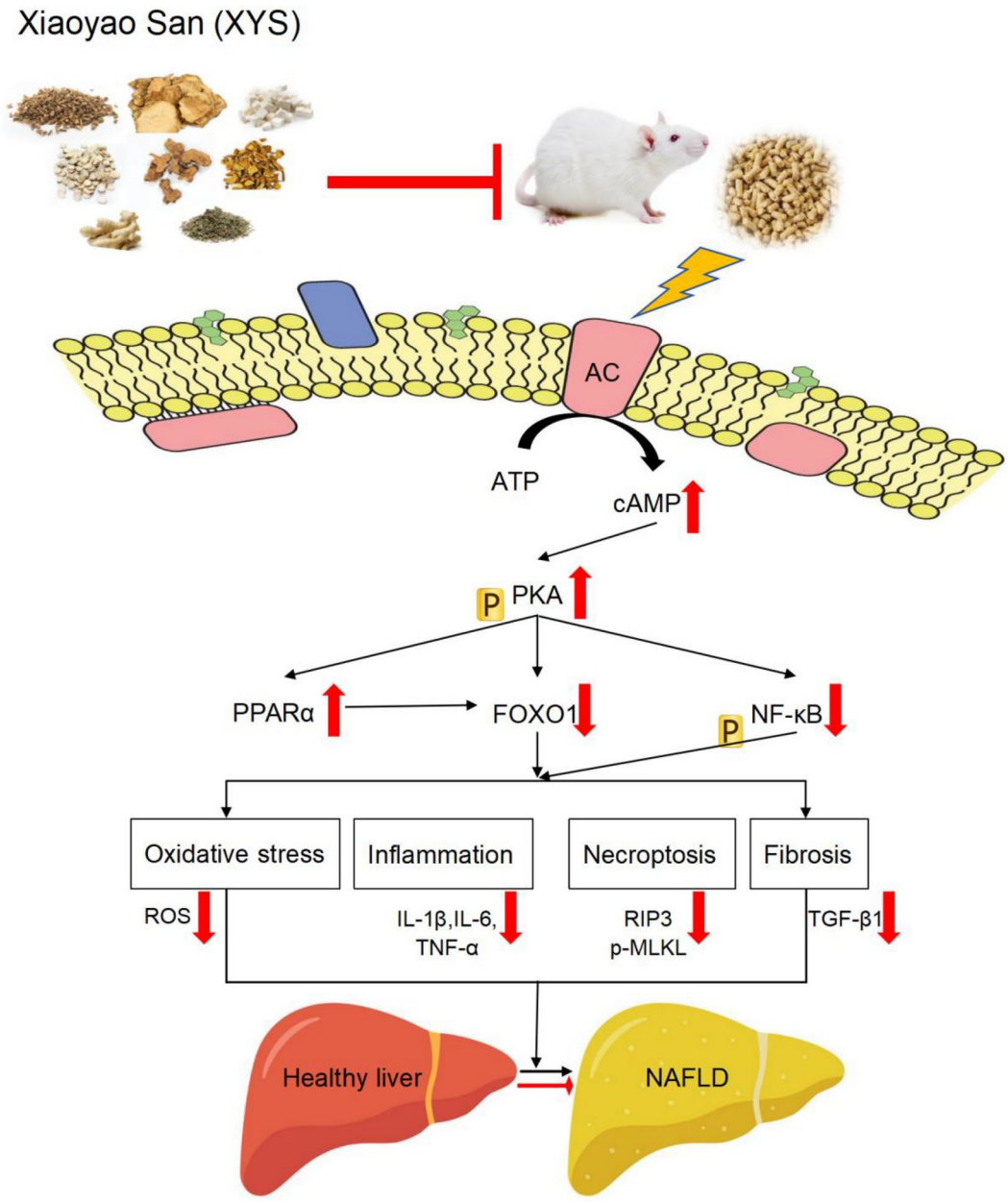

7

Fig. 9. Based on the integration of transcriptomics and proteomics analyses, the mechanism of XYS in the treatment of NAFLD. Schematic representation of the pathway retrieved from the KEGG database[19] (https://www.kegg.jp/). (KEGG Pathway ID: rno03320, rno04024, rno04068, rno04064).

inflammation. Given that hepatocytes are the primary cellular component of the liver, preventing hepatocyte necroptosis is crucial for delaying the progression of NAFLD[59], as it is associated with the development of liver fibrosis and the occurrence of cancer. RIP3 is a critical participant in the execution of necroptosis and an emerging metabolic regulator. By recruiting and phosphorylating MLKL, RIP3 induces changes in cell membrane permeability, leading to cell membrane rupture, necroptosis, and contributing to NAFLD-associated inflammation and cancer. The findings in this research align with conclusions from modern pharmacological studies. Furthermore, this research revealed that XYS intervention significantly altered liver tissue pathology in NAFLD model rats, regulating the expression of multiple proteins related to liver glucose and lipid metabolism (cAMP, PKA, FOXO1, and PPARα), inflammatory response (NF-κB), fibrosis (TGF-β1), and necroptosis (RIP3 and p-MLKL). This intervention enriched multiple KEGG pathways and identified PKA, PPARα, FOXO1, and NF-κB as core interconnected genes. The results further suggested that XYS inhibited the expression of NF-κB, p-NF-κB, FOXO1, TGF-β1, RIP3, and p-MLKL proteins in liver tissue, while upregulating the expression of cAMP, PKA, p-PKA, and PPARα proteins. These changes alleviated liver lipid accumulation, reduced inflammation and oxidative stress, and decreased liver fibrosis and necroptosis of hepatocytes. Collectively, these

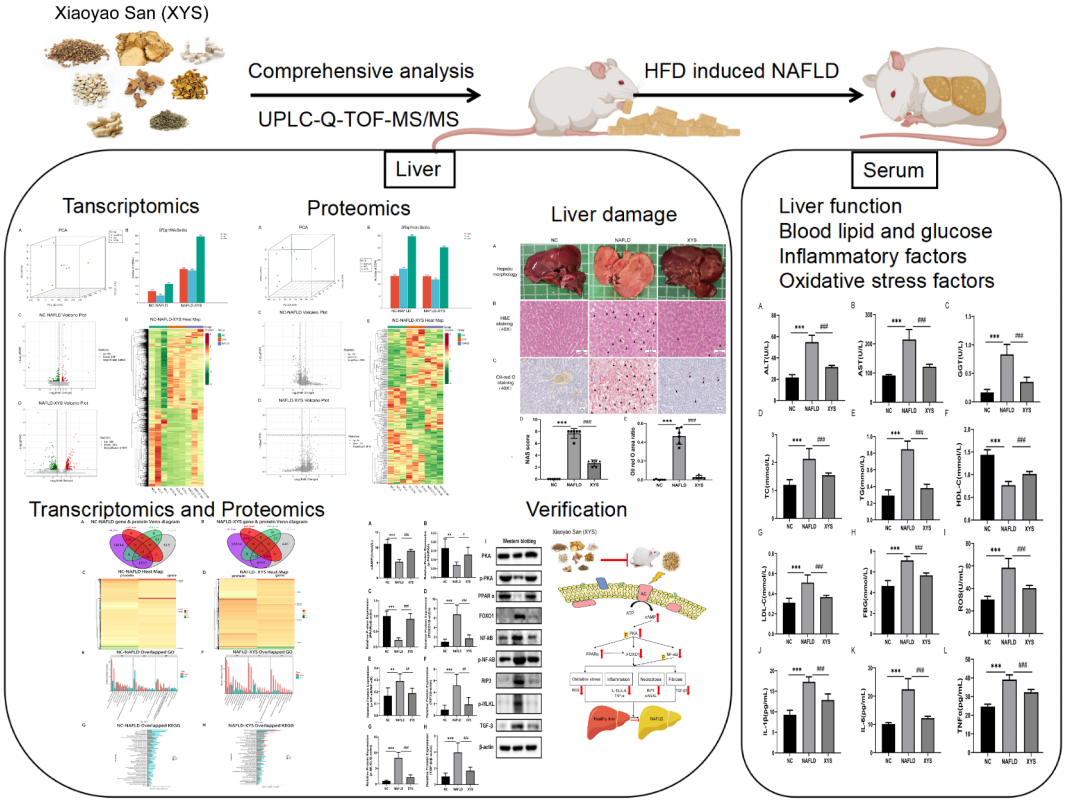

Fig. 10. The chemical analysis of XYS and its mechanism of action in NAFLD treatment.

findings deepen our understanding of the therapeutic mechanisms of XYS in NAFLD treatment. In conclusion, XYS attenuates HFD-induced lipid metabolism disorders, oxidative stress, inflammatory response, liver fibrosis, and necroptosis in NAFLD rats by regulating the cAMP/PKA-mediated PPARα, FOXO1, and NF-κB signaling pathways. In this study, we utilized an integrative analysis of transcriptomics and proteomics to elucidate the therapeutic mechanisms of XYS in treating NAFLD. Our findings demonstrated that XYS exerts significant therapeutic effects on NAFLD through multiple pathways, including inflammation, oxidative stress, lipid metabolism, and necroptosis. The study identifies PKA, PPARα, FOXO1, and NF-κB as potential therapeutic targets of XYS, which modulate the expression of downstream genes. This strategy, based on the combined analysis of transcriptomics and proteomics, provides a novel approach to elucidating the mechanisms of TCM formulas and deepens the scientific understanding of TCM theory. This research offers valuable insights for future investigations and contributes to the modernization of TCM research. Further studies are needed to fully explore the clinical potential of XYS in treating NAFLD.

In summary, this research comprehensively characterized the chemical composition of XYS and elucidated the targets and signaling pathways involved in its therapeutic mechanisms in NAFLD through integrated pharmaceutical chemical analysis, transcriptomics, and proteomics. The study identified 225 prototype chemical components of XYS that enter the bloodstream. The transcriptomics and proteomics analyses revealed that the therapeutic effect of XYS on NAFLD rat models primarily targets the cAMP, TGF-β, and NF-κB signaling pathways as well as necrotic apoptosis. Further validation confirmed that XYS suppresses the expression of NF-κB, p-NF-κB, FOXO1, TGF-β1, RIP3, and p-MLKL, while promoting the expression of cAMP, PKA, p-PKA, and PPARα in liver tissue. These findings indicate that XYS ameliorates NAFLD by regulating cAMP/PKA-mediated PPARα, FOXO1, and NF-κB signaling pathways. Therefore, this research provides valuable data and theoretical support for the potential application of XYS in NAFLD treatment, contributing to the scientific basis for using TCM in NAFLD therapy (Fig. 10).

Data availability

All data supporting the findings of this study are available within the article. The RNA-seq raw sequence data are available in NCBI short read archive (SRA) database under accession number PRJNA1183419. The mass spectrometry proteomics data have been deposited to the ProteomeXchange Consortium (https://proteomecentral.proteomexchange.org) with the dataset identifier PXD057729.

Received: 11 November 2024; Accepted: 24 February 2025
Published online: 26 March 2025

References

1. Estes, C., Razavi, H., Loomba, R., Younossi, Z. & Sanyal, A. J. Modeling the epidemic of nonalcoholic fatty liver disease demonstrates an exponential increase in burden of disease. *Hepatology* **67**, 123–133. https://doi.org/10.1002/hep.29466 (2018).
2. Shao, M. et al. Application of metabolomics in the diagnosis of non-alcoholic fatty liver disease and the treatment of traditional Chinese medicine. *Front. Pharmacol.* **13**, 971561. https://doi.org/10.3389/fphar.2022.971561 (2022).
3. Wang, L., Liu, X. E. & Zhuang, H. Research progress of omics biomarkers for nonalcoholic fatty liver disease. *Chin. J. Hepatol.* **29**, 604–608. https://doi.org/10.3760/cma.j.cn501113-20200708-00382 (2021).
4. Perakakis, N., Stefanakis, K. & Mantzoros, C. S. The role of omics in the pathophysiology, diagnosis and treatment of non-alcoholic fatty liver disease. *Metabolism* **111S**, 154320. https://doi.org/10.1016/j.metabol.2020.154320 (2020).
5. Nogales, C. et al. Network pharmacology: Curing causal mechanisms instead of treating symptoms. *Trends Pharmacol. Sci.* **43**, 136–150. https://doi.org/10.1016/j.tips.2021.11.004 (2022).
6. Zhou, Y. et al. Development of a novel anti-liver fibrosis formula with luteolin, licochalcone A, aloe-emodin and acacetin by network pharmacology and transcriptomics analysis. *Pharm. Biol.* **59**, 1594–1606. https://doi.org/10.1080/13880209.2021.1999275 (2021).
7. Lu, Y. et al. Dynamic network biomarker analysis and system pharmacology methods to explore the therapeutic effects and targets of Xiaoyaosan against liver cirrhosis. *J. Ethnopharmacol.* **294**, 115324. https://doi.org/10.1016/j.jep.2022.115324 (2022).
8. Hu, T. et al. Xiaoyao San attenuates hepatic steatosis through estrogen receptor α pathway in ovariectomized ApoE-/- mice. *J. Ethnopharmacol.* **282**, 114612. https://doi.org/10.1016/j.jep.2021.114612 (2022).
9. Chen, M. et al. Investigating the mechanisms of Modified Xiaoyaosan in suppressing the progression of atherosclerosis, by means of integrative pharmacology and experimental validation. *Aging* **13**, 11411–11432. https://doi.org/10.18632/aging.202832 (2021).
10. Bai, Z. et al. Xiao-Yao-San protects against anti-tuberculosis drug-induced liver injury by regulating Grsf1 in the mitochondrial oxidative stress pathway. *Front. Pharmacol.* **13**, 948128. https://doi.org/10.3389/fphar.2022.948128 (2022).
11. Zhang, Z. et al. Xiaoyaosan slows cancer progression and ameliorates gut dysbiosis in mice with chronic restraint stress and colorectal cancer xenografts. *Biomed. Pharmacother.* **132**, 110916. https://doi.org/10.1016/j.biopha.2020.110916 (2020).
12. Zhou, Y. et al. Xiaoyaosan decoction alleviated rat liver fibrosis via the TGFβ/Smad and Akt/$FoxO_3$ signaling pathways based on network pharmacology analysis. *J. Ethnopharmacol.* **264**, 113021. https://doi.org/10.1016/j.jep.2020.113021 (2021).
13. Liu, Q. et al. Efficacy and safety of chinese herbal medicine Xiao Yao San in functional gastrointestinal disorders: A meta-analysis and trial sequential analysis of randomized controlled trials. *Front. Pharmacol.* **12**, 821802. https://doi.org/10.3389/fphar.2021.821802 (2022).
14. Zhong, M. et al. Astragalus mongholicus polysaccharides ameliorate hepatic lipid accumulation and inflammation as well as modulate gut microbiota in NAFLD rats. *Food Funct.* **13**, 7287–7301. https://doi.org/10.1039/d2fo01009g (2022).
15. Uehara, K. et al. Activation of liver mTORC1 protects against NASH via dual regulation of VLDL-TAG secretion and De Novo lipogenesis. *Cell Mol. Gastroenterol. Hepatol.* **13**, 1625–1647. https://doi.org/10.1016/j.jcmgh.2022.02.015 (2022).
16. Bjørnå, et al. Prevalence and risk factors of nonalcoholic fatty liver disease in a general population, the HUNT study. *Scand. J. Gastroenterol.* **58**, 505–511. https://doi.org/10.1080/00365521.2022.2139633 (2023).
17. Li, C. X. et al. Allyl isothiocyanate ameliorates lipid accumulation and inflammation in nonalcoholic fatty liver disease via the Sirt1/AMPK and NF-κB signaling pathways. *World J. Gastroenterol.* **25**, 5120–5133. https://doi.org/10.3748/wjg.v25.i34.5120 (2019).
18. Tao, S., Yang, Y., Li, J., Wang, H. & Ma, Y. Bixin attenuates high-fat diet-caused liver steatosis and inflammatory injury through Nrf2/PPARα signals. *Oxid. Med. Cell Longev.* **2021**, 6610124. https://doi.org/10.1155/2021/6610124 (2021).
19. Kanehisa, M., Furumichi, M., Sato, Y., Matsuura, Y. & Ishiguro-Watanabe, M. KEGG: Biological systems database as a model of the real world. *Nucleic Acids Res.* **53**, D672–D677. https://doi.org/10.1093/nar/gkae909 (2025).
20. Li, Z. et al. Liraglutide protects against inflammatory stress in non-alcoholic fatty liver by modulating Kupffer cells M2 polarization via cAMP-PKA-STAT3 signaling pathway. *Biochem. Biophys. Res. Commun.* **510**, 20–26. https://doi.org/10.1016/j.bbrc.2018.12.149 (2019).
21. Lazarus, J. V. et al. NAFLD—Sounding the alarm on a silent epidemic. *Nat. Rev. Gastroenterol. Hepatol.* **17**, 377–379. https://doi.org/10.1038/s41575-020-0315-7 (2020).
22. Shen, S., Wang, K., Zhi, Y., Shen, W. & Huang, L. Gypenosides improves nonalcoholic fatty liver disease induced by high-fat diet induced through regulating LPS/TLR4 signaling pathway. *Cell Cycle* **19**, 3042–3053. https://doi.org/10.1080/15384101.2020.1829800 (2020).
23. Yao, Q. et al. Yin Zhi Huang, a traditional Chinese herbal formula, ameliorates diet-induced obesity and hepatic steatosis by activating the AMPK/SREBP-1 and the AMPK/ACC/CPT1A pathways. *Ann. Transl. Med.* **8**, 231. https://doi.org/10.21037/atm.2020.01.31 (2020).
24. Xu, H. Y. et al. Sesamol alleviates obesity-related hepatic steatosis via activating hepatic PKA pathway. *Nutrients* **12**, 329. https://doi.org/10.3390/nu12020329 (2020).
25. Tian, J. et al. JianPi-QingHua formula attenuates nonalcoholic fatty liver disease by regulating the AMPK/SIRT1/NF-κB pathway in high-fat-diet-fed C57BL/6 mice. *Pharm. Biol.* **61**, 647–656. https://doi.org/10.1080/13880209.2023.2188549 (2023).
26. Liu, X. J. et al. Characterization of a murine nonalcoholic steatohepatitis model induced by high fat high calorie diet plus fructose and glucose in drinking water. *Lab Invest.* **98**, 1184–1199. https://doi.org/10.1038/s41374-018-0074-z (2018).
27. Zhang, J. & Feng, Q. Pharmacological effects and molecular protective mechanisms of astragalus polysaccharides on nonalcoholic fatty liver disease. *Front. Pharmacol.* **13**, 854674. https://doi.org/10.3389/fphar.2022.854674 (2022).
28. Liu, N. et al. Xiaoyao Powder in the treatment of non-alcoholic fatty liver disease: A systematic review and meta-analysis. *J. Ethnopharmacol.* **288**, 114999. https://doi.org/10.1016/j.jep.2022.114999 (2022).
29. Zhao, W., Feng, X., Liu, B., Xian, J. & Zhang, N. Er-miao-fang extracts inhibits adipose lipolysis and reduces hepatic gluconeogenesis via suppression of inflammation. *Front. Physiol.* **9**, 1041. https://doi.org/10.3389/fphys.2018.01041 (2018).
30. Wahlang, B., McClain, C., Barve, S. & Gobejishvili, L. Role of cAMP and phosphodiesterase signaling in liver health and disease. *Cell Signal* **49**, 105–115. https://doi.org/10.1016/j.cellsig.2018.06.005 (2018).
31. Yang, J. et al. Hepatic PKA inhibition accelerates the lipid accumulation in liver. *Nutr. Metab. (Lond).* **16**, 69. https://doi.org/10.1186/s12986-019-0400-5 (2019).
32. Hong, E., Kang, H., Yang, G., Oh, S. & Kim, E. The PKA-SREBP1c pathway plays a key role in the protective effects of lactobacillus johnsonii JNU3402 against diet-induced fatty liver in mice. *Mol. Nutr. Food Res.* **67**, e2200496. https://doi.org/10.1002/mnfr.202200496 (2023).
33. Zingg, J. M. et al. Modulation of cAMP levels by high-fat diet and curcumin and regulatory effects on CD36/FAT scavenger receptor/fatty acids transporter gene expression. *Biofactors* **43**, 42–53. https://doi.org/10.1002/biof.1307 (2017).
34. Kou, X. H. et al. Bilobetin ameliorates insulin resistance by PKA-mediated phosphorylation of PPARα in rats fed a high-fat diet. *Br. J. Pharmacol.* **165**, 2692–2706. https://doi.org/10.1111/j.1476-5381.2011.01727.x (2012).
35. Ren, L. et al. Chronic treatment with the modified Longdan Xiegan Tang attenuates olanzapine-induced fatty liver in rats by regulating hepatic de novo lipogenesis and fatty acid beta-oxidation-associated gene expression mediated by SREBP-1c, PPAR-alpha and AMPK-alpha. *J. Ethnopharmacol.* **232**, 176–187. https://doi.org/10.1016/j.jep.2018.12.034 (2019).
36. Boonloh, K., Thanaruksa, R., Proongkhong, T., Thawornchinsombut, S. & Pannangpetch, P. Nil-surin rice bran hydrolysates improve lipid metabolism and hepatic steatosis by regulating secretion of adipokines and expression of lipid-metabolism genes. *J. Med. Food* **25**, 597–606. https://doi.org/10.1089/jmf.2021.K.0170 (2022).

37. Cariello, M., Piccinin, E. & Moschetta, A. Transcriptional regulation of metabolic pathways via lipid-sensing nuclear receptors PPARs, FXR, and LXR in NASH. *Cell Mol. Gastroenterol. Hepatol.* **11**, 1519–1539. https://doi.org/10.1016/j.jcmgh.2021.01.012 (2021).
38. Sun, N. et al. Hepatic Krüppel-like factor 16 (KLF16) targets PPARα to improve steatohepatitis and insulin resistance. *Gut* **70**, 2183–2195. https://doi.org/10.1136/gutjnl-2020-321774 (2021).
39. Sandoval-Rodriguez, A. et al. Pirfenidone is an agonistic ligand for PPARα and improves NASH by activation of SIRT1/LKB1/pAMPK. *Hepatol. Commun.* **4**, 434–449. https://doi.org/10.1002/hep4.1474 (2020).
40. Zhang, C. H. et al. Gegen Qinlian Decoction abates nonalcoholic steatohepatitis associated liver injuries via anti-oxidative stress and anti-inflammatory response involved inhibition of toll-like receptor 4 signaling pathways. *Biomed. Pharmacother.* **126**, 110076. https://doi.org/10.1016/j.biopha.2020.110076 (2020).
41. Gong, X., Li, T., Wan, R. & Sha, L. Cordycepin attenuates high-fat diet-induced non-alcoholic fatty liver disease via down-regulation of lipid metabolism and inflammatory responses. *Int. Immunopharmacol.* **91**, 107173. https://doi.org/10.1016/j.intimp.2020.107173 (2021).
42. Zhang, W., Sun, Y., Liu, W., Dong, J. & Chen, J. SIRT1 mediates the role of RNA-binding protein QKI 5 in the synthesis of triglycerides in non-alcoholic fatty liver disease mice via the PPARα/FoxO1 signaling pathway. *Int. J. Mol. Med.* **43**, 1271–1280. https://doi.org/10.3892/ijmm.2019.4059 (2019).
43. Wu, Y. et al. Novel mechanism of Foxo1 phosphorylation in glucagon signaling in control of glucose homeostasis. *Diabetes* **67**, 2167–2182. https://doi.org/10.2337/db18-0674 (2018).
44. Tao, R. et al. Hepatic FoxOs regulate lipid metabolism via modulation of expression of the nicotinamide phosphoribosyltransferase gene. *J. Biol. Chem.* **286**, 14681–14690. https://doi.org/10.1074/jbc.M110.201061 (2011).
45. Dumeus, S. et al. Bioactive peptide improves diet-induced hepatic fat deposition and hepatocyte proinflammatory response in SAMP8 ageing mice. *Cell. Physiol. Biochem.* **48**, 1942–1952. https://doi.org/10.1159/000492518 (2018).
46. Sabir, U., Irfan, H. M., Alamgeer, I. U., Niazi, Z. R. & Asjad, H. M. M. Phytochemicals targeting NAFLD through modulating the dual function of forkhead box O1 (FOXO1) transcription factor signaling pathways. *Naunyn-Schmiedebergs Arch. Pharmacol.* **395**(7), 741–755. https://doi.org/10.1007/s00210-022-02234-2 (2022).
47. Wang, Y. et al. Regulation of SIRT3/FOXO1 signaling pathway in rats with non-alcoholic steatohepatitis by salvianolic acid B. *Arch. Med. Res.* **48**, 506–512. https://doi.org/10.1016/j.arcmed.2017.11.016 (2017).
48. Ding, H. R. et al. Protective properties of FOXO1 inhibition in a murine model of non-alcoholic fatty liver disease are associated with attenuation of ER stress and necroptosis. *Front. Physiol.* **11**, 177. https://doi.org/10.3389/fphys.2020.001772020;11:177 (2020).
49. Zhao, N. et al. Palmitate induces fat accumulation via repressing FoxO1-mediated ATGL-dependent lipolysis in HepG2 hepatocytes. *PloS one* **16**, e0243938. https://doi.org/10.1371/journal.pone.0243938 (2021).
50. Pan, Q. et al. Hepatocyte FoxO1 deficiency protects from liver fibrosis via reducing inflammation and TGF-β1-mediated HSC activation. *Cell. Mol. Gastroenterol. Hepatol.* **17**, 41–58. https://doi.org/10.1016/j.jcmgh.2023.08.013 (2024).
51. Zou, H. et al. Hippophae rhamnoides reverses decreased CYP2D6 expression in rats with BCG-induced liver injury. *Sci. Rep.* **13**, 17425. https://doi.org/10.1038/s41598-023-44590-w (2023).
52. Ke, B. et al. Inactivation of NF-κB p65 (RelA) in liver improves insulin sensitivity and inhibits cAMP/PKA pathway. *Diabetes* **64**, 3355–3362. https://doi.org/10.2337/db15-0242 (2015).
53. Didamoony, M. A., Atwa, A. M. & Ahmed, L. A. A novel mechanistic approach for the anti-fibrotic potential of rupatadine in rat liver via amendment of PAF/NF-κB p65/TGF-β1 and hedgehog/HIF-1α/VEGF trajectories. *Inflammopharmacology* **31**, 845–858. https://doi.org/10.1007/s10787-023-01147-7 (2023).
54. Shi, Y. et al. Filamin A facilitates NLRP3 inflammasome activation during arsenic-induced nonalcoholic steatohepatitis. *Environ. Sci. Pollut. Res. Int.* **30**, 107703–107715. https://doi.org/10.1007/s11356-023-29702-3 (2023).
55. Zhao, W. et al. Myristica fragrans extract regulates gut microbes and metabolites to attenuate hepatic inflammation and lipid metabolism disorders via the AhR-FAS and NF-κB signaling pathways in mice with non-alcoholic fatty liver disease. *Nutrients* **14**, 1699. https://doi.org/10.3390/nu14091699 (2022).
56. Guo, F. et al. Green pea (*Pisum sativum* L.) Hull polyphenol extract alleviates NAFLD through VB6/TLR4/NF-κB and PPAR pathways. *J. Agric. Food Chem.* **71**, 16067–16078. https://doi.org/10.1021/acs.jafc.3c02337 (2023).
57. Aoyama, Y. et al. Lactoferrin prevents hepatic injury and fibrosis via the inhibition of NF-κB signaling in a rat non-alcoholic steatohepatitis model. *Nutrients* **14**, 42. https://doi.org/10.3390/nu14010042 (2021).
58. Wei, Z. et al. Ferulic acid attenuates non-alcoholic steatohepatitis by reducing oxidative stress and inflammation through inhibition of the ROCK/NF-κB signaling pathways. *J. Pharmacol. Sci.* **147**, 72–80. https://doi.org/10.1016/j.jphs.2021.05.006 (2021).
59. Zhang, H. et al. Intermittent hypoxia aggravates non-alcoholic fatty liver disease via RIPK3-dependent necroptosis-modulated Nrf2/NFκB signaling pathway. *Life Sci.* **285**, 119963. https://doi.org/10.1016/j.lfs.2021.119963 (2021).

Author contributions

Yunxiao Liu:Conceptualization, Methodology, Software, Investigation, Formal Analysis, Writing—Original Draft,Revision; Shuanghu Wang: Visualization, Investigation,Revision; Ayesha Younas:Revision,Funding acquisition; Jiaojian Lv:Resources, Supervision, Validation,Revision; Abdullah Al Mamun: Data Curation; Chuxiao Shao: Visualization, Writing—Review and Editing;Funding acquisition.

Funding

This study was partially supported by the funds from the Key Research and Development Program of Zhejiang Province (2024C03171), the Key Research and Development Project of Lishui (2023zdyf15).

Competing interests

The authors declare no competing interests.

Additional information

Supplementary Information The online version contains supplementary material available at https://doi.org/10.1038/s41598-025-91890-4.

Correspondence and requests for materials should be addressed to C.S.